

Structural, Magnetic and Electrical Properties of Nd³⁺-Doped PbWO₄ Ceramic Materials

B. SAWICKI^a, E. TOMASZEWICZ^b, T. GRON^{a,*},
M. OBOZ^a, P. ZAJDEL^a, I. GRUSZKA^a,
A. GUZIK^a AND P. URBANOWICZ^a

^a*Institute of Physics, University of Silesia in Katowice, 40-007 Katowice, Poland*

^b*Faculty of Chemical Technology and Engineering, West Pomeranian University of Technology in Szczecin, 70-310 Szczecin, Poland*

Doi: [10.12693/APhysPolA.142.629](https://doi.org/10.12693/APhysPolA.142.629)

*e-mail: tadeusz.gron@us.edu.pl

Sub-microcrystalline samples of Pb_{1-3x}□_xNd_{2x}WO₄ (PbNdW) solid solution ($x = 0.0098, 0.0455, 0.0839, \text{ and } 0.1667$, where □ denotes vacant sites) prepared by citrate-nitrate combustion method were pressed and sintered at 1050°C to a ceramic form. Therefore, it is expected that the ceramics under study display also unique properties and new potential applications. This paper presents the results of structural, microscopic, magnetic, and electrical, as well as broadband dielectric spectroscopy measurements of PbNdW ceramic samples with a scheelite-type structure. The studies showed that replacing diamagnetic Pb²⁺ ions with paramagnetic Nd³⁺ ones possessing a screened 4*f*-shell leads to greater charge accumulation capacity, higher relative electric permittivity, low energy losses, and suppression of dipole relaxation. The important result of the transformation of sub-microcrystalline samples into ceramics is an increase in dielectric permittivity with a simultaneous reduction in electrical conductivity.

topics: ceramics, magnetic properties, electrical conductivity, dielectric spectroscopy

1. Introduction

Lead tungstate (PbWO₄) is a very popular scintillating material used in the generation of high-energy physics, especially important for newly designed instruments for use in the Large Hadron Collider (at CERN) [1, 2]. At room temperature, lead tungstate presents a scheelite-type tetragonal structure belonging to the *I*4₁/*a* space group [2]. RE³⁺-doped PbWO₄ powders and single crystals exhibit good photoluminescence and are promising laser materials [3].

Based on the lead tungstate matrix, we have obtained many RE³⁺-doped materials by solid state and combustion methods. Interesting results were given in studies of broadband dielectric spectroscopy of solid solution Pb_{1-3x}□_xGd_{2x}(MoO₄)_{1-3x}(WO₄)_{3x} synthesized by both high-temperature sintering [4] and combustion method [5], which in the first case showed faster and slower relaxation processes in different time scales, while in the second case, the dipole relaxation disappeared as the grain size decreased, causing the spatial polarization to appear.

We present the results of structural, microscopic, magnetic, and electrical studies of Pb_{1-3x}□_xNd_{2x}WO₄ (labeled later as PbNdW) lead

tungstates that have been successfully obtained by combustion route and then sintered to a ceramic form, expecting that ceramic samples will have a wider application in electronic technology than materials with smaller grain sizes.

2. Experimental details

Sub-microcrystalline samples of solid solution with the chemical formula of Pb_{1-3x}□_xNd_{2x}WO₄ ($x = 0.0098, 0.0455, 0.0839, \text{ and } 0.1667$) obtained via combustion route were pressed into pellets



Fig. 1. Image of ceramic pastille after technological processing. The length of the grille is 5 mm.

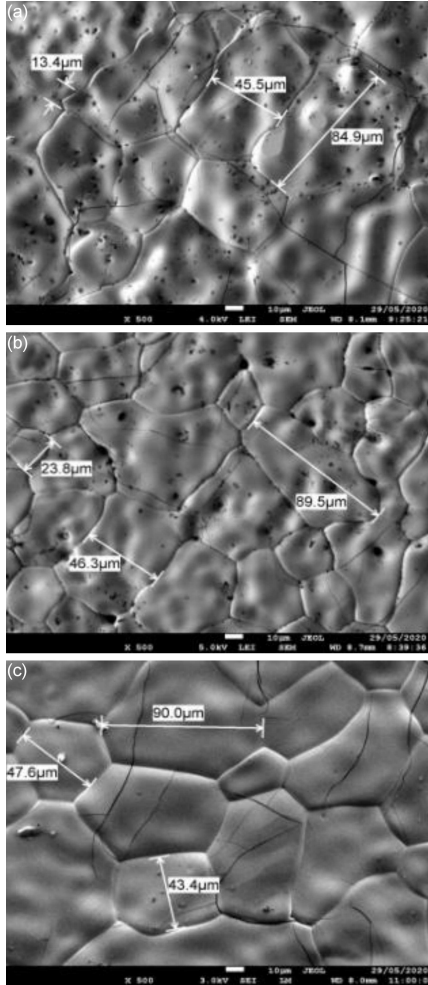


Fig. 2. SEM images of PbNdW ceramic samples when $x = 0.0455$ (a), $x = 0.0839$ (b), and $x = 0.1667$ (c). Magnification $\times 500$.

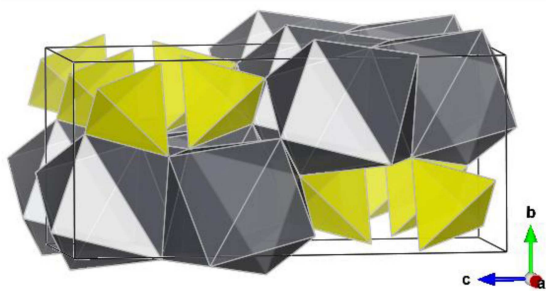


Fig. 3. Projection of stolite structure along the a-axis. Structure is built of twin chains of corner sharing (WO_4) tetrahedra and edge-sharing (PbO_8) polyhedra.

for magnetic and electrical studies. Next, they were crushed and ground in an agate mortar, and powders were pressed again in a matrix with a diameter of 12 mm and a pressure of $p = 19$ MPa. The samples prepared this way were placed in an alumina crucible and then sintered at 1050°C

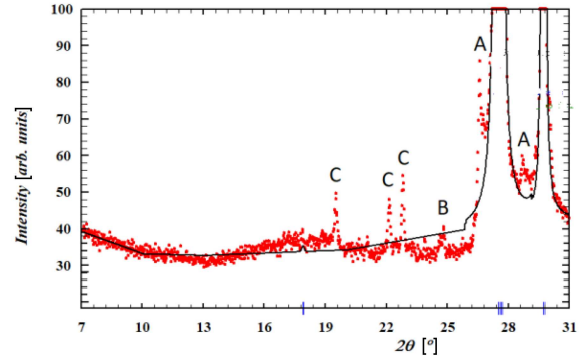


Fig. 4. Low-angle section presenting additional reflections and lack of superstructure expected for vacancy ordered derivatives [11] with reflections under $2\theta = 16^\circ$ of PbNdW ($x = 0.0455$) ceramic sample. Other assigned reflections: A — tube tail peaks, B — Cu K_β , C — unidentified impurities.

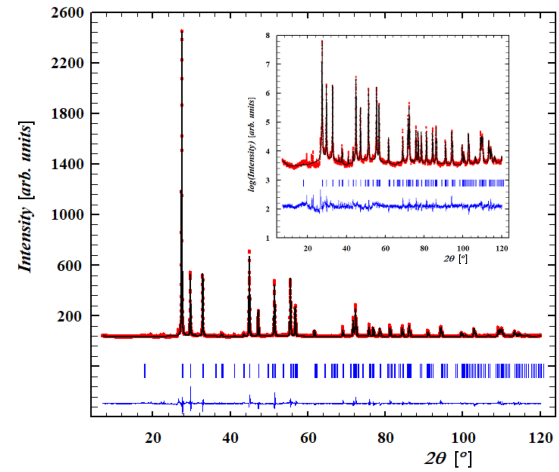


Fig. 5. Plot of the Rietveld refinement of PbNdW ($x = 0.0455$) ceramic sample presented on a linear scale with an inset plotted on a logarithmic scale.

for 12 h in a VMK 1600 furnace (Linn High Therm GmbH, Hirschbach-Eschenfelden, Germany). After such technological treatment, the samples had a ceramic consistency (Fig. 1). Morphology of Nd^{3+} -doped materials and their elemental composition were conducted using a JEOL JSM-7600F scanning electron microscope (SEM) equipped with the X-max Oxford energy dispersive X-ray spectroscopy (EDS) microprobe (Fig. 2).

X-ray powder diffraction measurements were carried out on a PANalytical PW1050 diffractometer using a nickel-filtered Cu $K_{\alpha 1,2}$ source operating at 30 kV/30 mA. Each ceramic sample was ground in an agate mortar and deposited on a double-sided scotch tape attached to a glass slide. Powder diffraction patterns were collected in the 2θ range from 7 to 120° with the 0.02° step and 36 s per step. The X-ray beam spilled over the sample under 17° which was later corrected in the refinement.

TABLE I

Magnetic parameters of PbNdW tungstates: C is the Curie constant, Θ is the Curie–Weiss temperature, μ_{eff} is the effective magnetic moment, M is the magnetization at 2 K and in the magnetic field of 70 kOe, p_{eff} is the effective number of Bohr magnetons, M_0 is the magnetization at the highest value of H/T , and g is the Landé factor.

x	Experiment				p_{eff}	Brillouin fit	
	C [emu K/mol]	Θ [K]	μ_{eff} [μ_B /f.u.]	M [μ_B /f.u.]		M_0 [μ_B /f.u.]	g
0.0098	0.053	−63.0	0.648	0.027	0.358	0.028	0.70
0.0455	0.112	−12.4	0.948	0.117	0.772	0.123	0.69
0.0839	0.252	−24.2	1.419	0.209	1.048	0.224	0.60
0.1667	0.526	−29.2	2.052	0.418	1.477	0.450	0.59

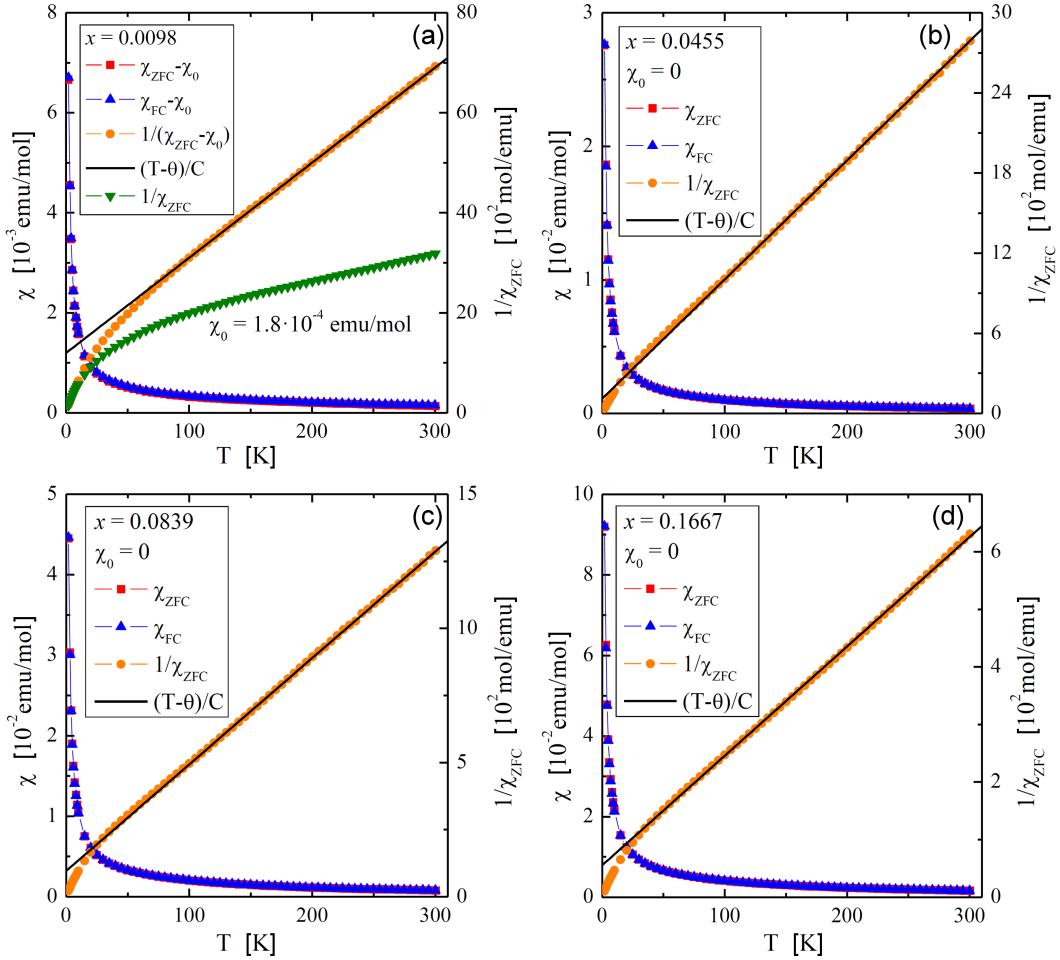


Fig. 6. ZFC and FC DC magnetic susceptibility χ as well as $1/\chi_{ZFC}$ vs temperature T of PbNdW tungstates for $x = 0.0098$ (a), 0.0455 (b), 0.0839 (c), and 0.1667 (d) at $H_{DC} = 1$ kOe. The solid (black) line, $(T - \Theta)/C$, indicates a Curie–Weiss behavior and χ_0 represents all temperature independent susceptibilities [14].

The main phase was identified by a visual inspection based on data available in the literature [6] and in the Crystallography Open Database. A starting model was based on stolzite (PbWO_4), with scheelite-type (Fig. 3) tetragonal structure ($I41/a$, SG No. 88), as was reported earlier [7–9]. Several additional reflections were observed (Fig. 4), and their origins were verified versus a possible

presence of a metastable monoclinic ($P21/a$) raspite (PbWO_4) [10], different lead or tungsten oxides [6], or vacancy-ordered structures [11]. An additional search for a different superstructure up to $3 \times 3 \times 3$ cell was also negative. The Rietveld refinement [12] was carried out with the FullProf software suite [13] using nominal stoichiometry and ionic form factors (Fig. 5). The refined

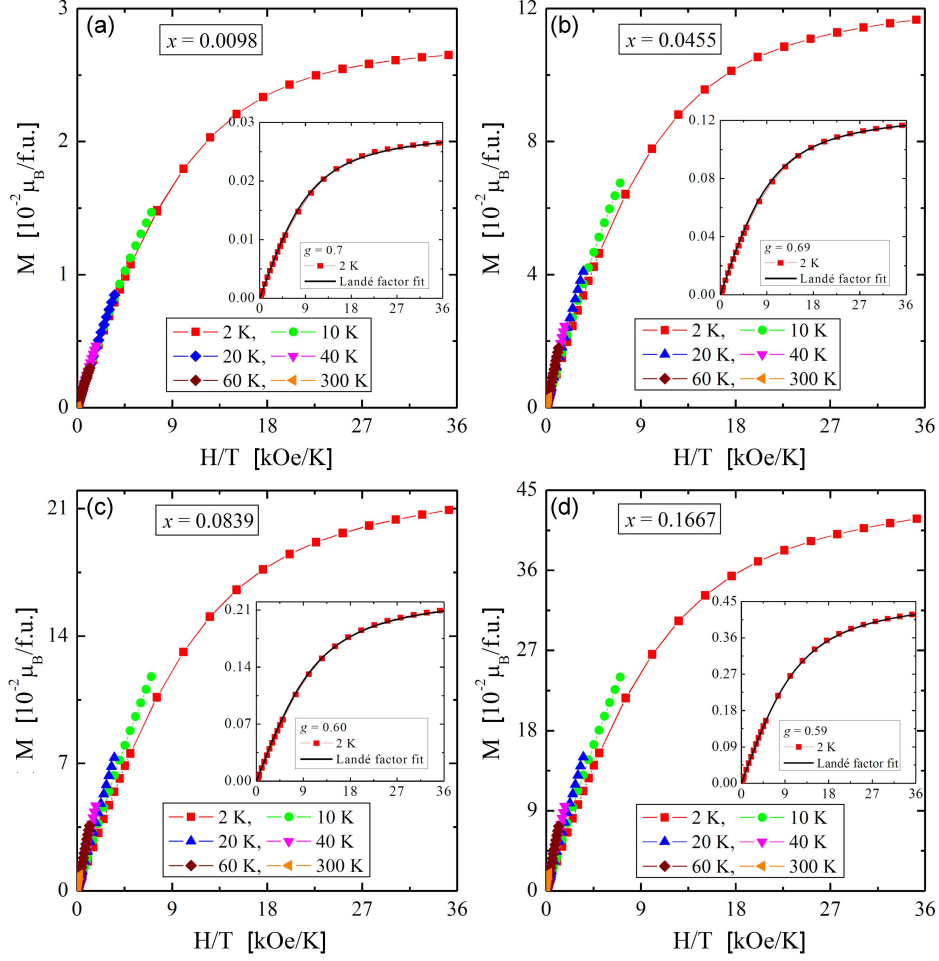


Fig. 7. Magnetization M vs H/T of PbNdW tungstates for $x = 0.0098$ (a), 0.0455 (b), 0.0839 (c), and 0.1667 (d) at 2, 10, 20, 40, 60, and 300 K. Inset: Landé factor fit (solid black line) to the experimental data at 2 K.

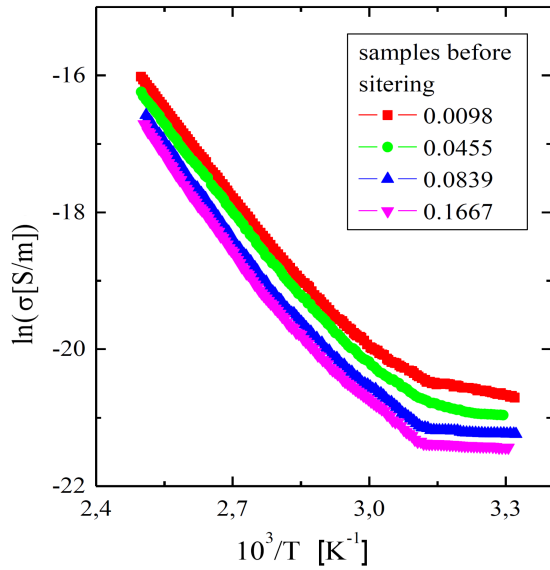


Fig. 8. Electrical conductivity ($\ln \sigma$) vs reciprocal temperature $10^3/T$ of PbNdW samples before sintering, when $x = 0.0098$, 0.0455 , 0.0839 , and 0.1667 .

crystallographic parameters for PbNdW ceramic sample when $x = 0.0455$ are: lattice parameters $a = 5.4389(1) \text{ \AA}$ and $c = 12.0148(1) \text{ \AA}$, cell volume $V = 355.42(1) \text{ \AA}^3$, crystallographic density 8.22 g/cm^3 , atomic Wyckoff positions W (4a) $(1/2, 1/4, 3/8)$, Pb/Nd (4b) $(0, 3/4, 3/8)$, O (16f) $(0.634(2), 0.023(2), 0.289(8))$, common isotropic atomic displacement parameter ADP $0.51(2) \text{ \AA}^2$.

Magnetic susceptibility, both in ZFC (zero-field-cooled) and FC (field-cooled) mode, and magnetization were measured in the temperature range of 2–300 K using a Quantum Design MPMS-XL-7AC SQUID magnetometer (USA). The electrical conductivity was measured by a DC (direct current) method using a KEITHLEY 6517B electrometer/high-resistance meter (USA). Broadband dielectric spectroscopy measurements were carried out using pellets, polished and sputtered with ($\sim 80 \text{ nm}$) Ag electrodes in the frequency range from 200 Hz to 1 MHz with an LCR HiTESTER 3532-50 (HIOKI, Japan) within the temperature range of 79–400 K. For electrical measurements the electrical and thermal contacts were made with a silver lacquer mixture.

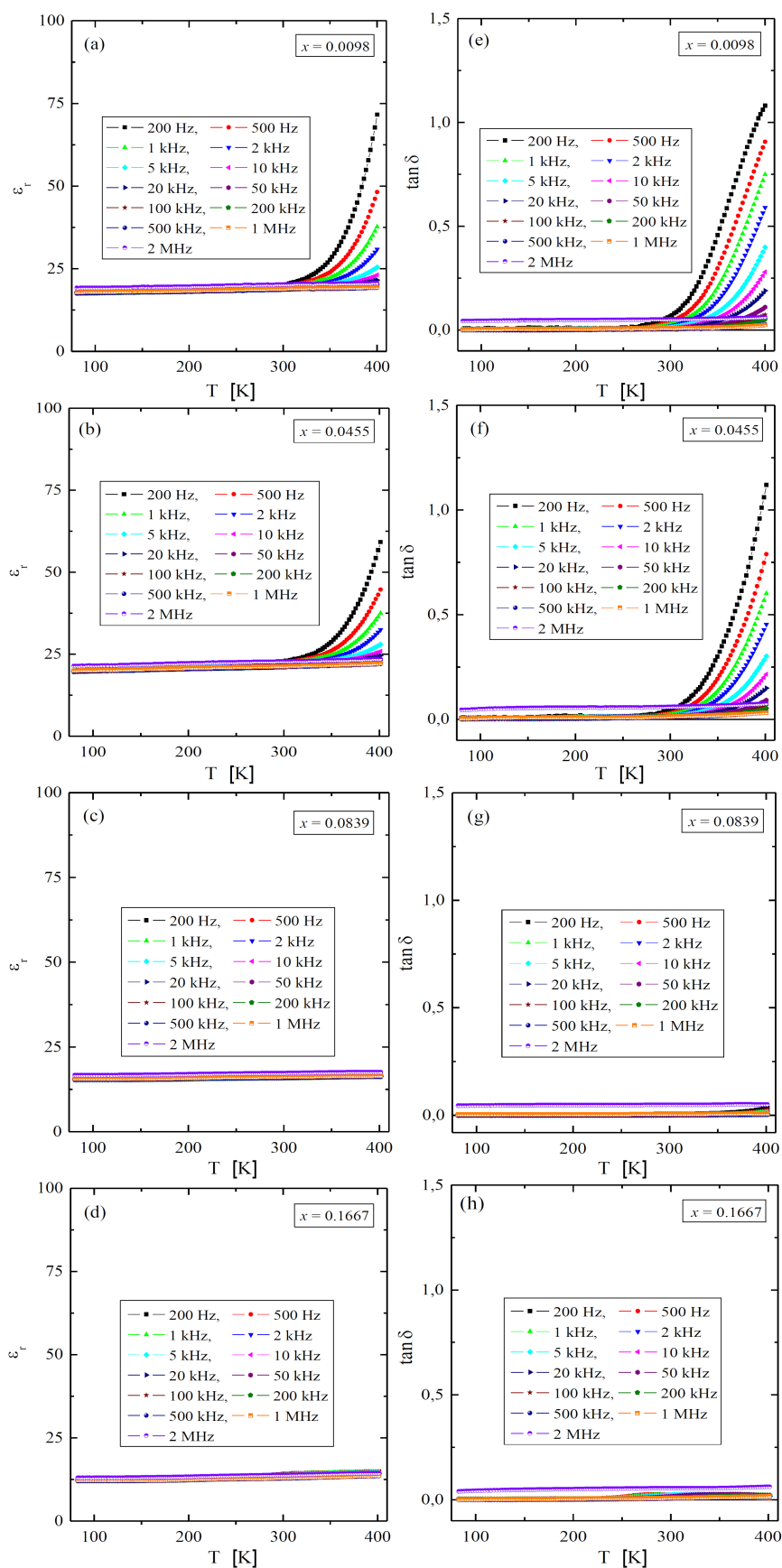


Fig. 9. Relative permittivity ϵ_r (a)–(d) and loss tangent $\tan \delta$ (e)–(h) vs temperature T of PbNdW samples before sintering in the frequency range of 200 Hz–2 MHz for $x = 0.0098, 0.0455, 0.0839, 0.1667$.

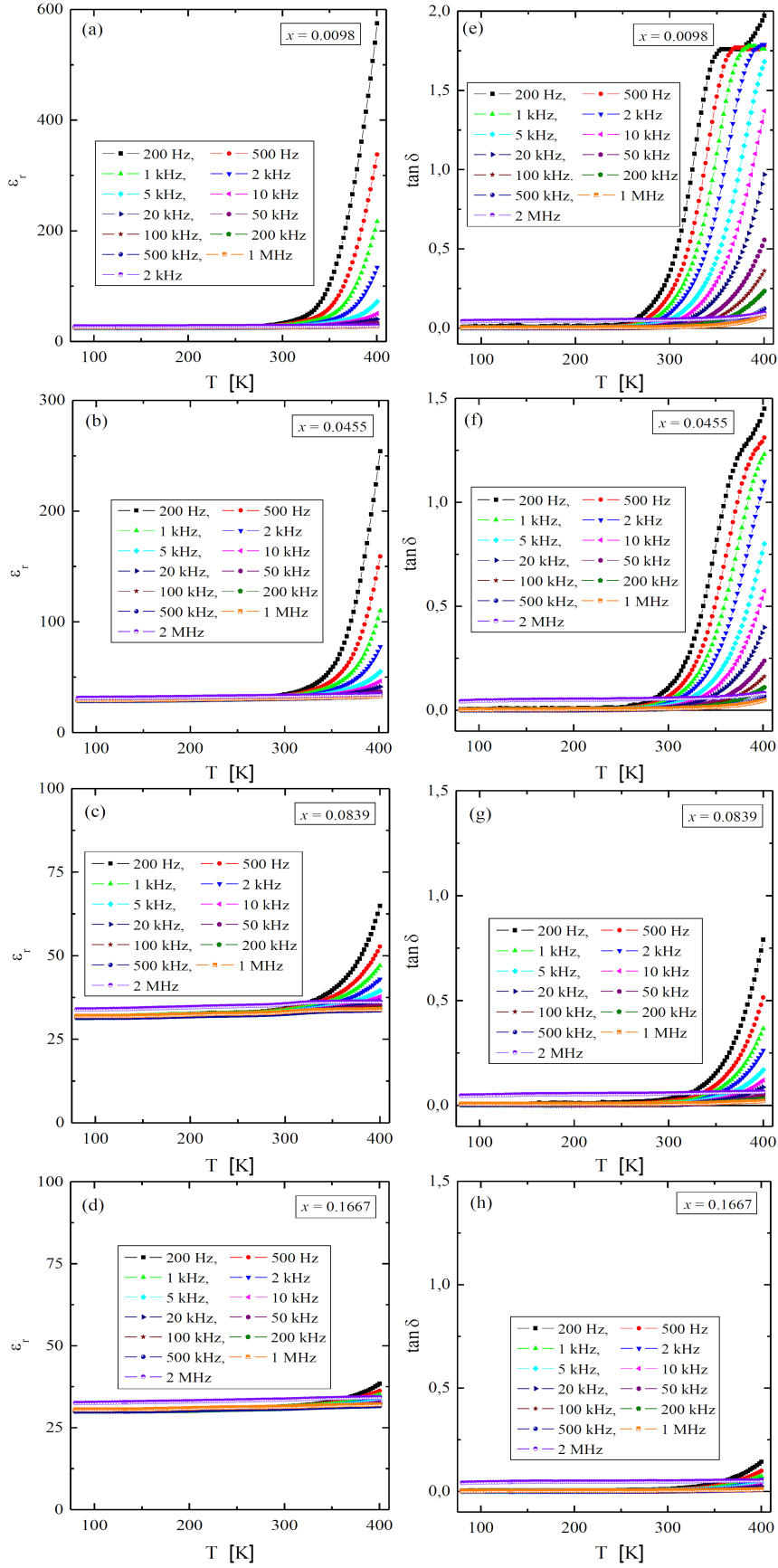


Fig. 10. Relative permittivity ϵ_r (a-d) and loss tangent $\tan \delta$ (e-h) vs temperature T of PbNdW ceramic samples in the frequency range of 200 Hz–2 MHz for $x = 0.0098, 0.0455, 0.0839, 0.1667$.

3. Results and discussion

3.1. X-ray diffraction studies

Powder X-ray diffraction studies confirmed that the materials crystallized in a tetragonal unit cell with the space group ($I41/a$, SG No. 88) [7–9]. The possible lowering of symmetry reported earlier by Moreau [2] should leave a traceable signature in the low-angle part of the patterns, which is not observed in the current experiment. Due to the stoichiometry enforced by charge balance requirements, the materials possess intrinsic cation vacancies, which offers a chance for vacancy ordering. However, the three peaks marked as C in Fig. 4 cannot be refined with a supercell up to $3 \times 3 \times 3$ limit. Therefore, they are considered to be impurities, but a further study of a single crystal might be required to conclusively answer this question. The patterns were also inspected with respect to a possible presence of a monoclinic raspite phase [10], in which stronger reflections should appear at 13.7 and $16.7^\circ 2\theta$. No intensities above the background were detected in these locations, excluding this possibility.

3.2. Magnetic properties

The results of magnetic susceptibility and magnetization isotherm measurements of PbNdW tungstates ($x = 0.0098, 0.0455, 0.0839, \text{ and } 0.1667$) are depicted in Figs. 6 and 7, respectively, and in Table I. All Nd^{3+} -doped tungstates are paramagnetic in the temperature range of 2–300 K and have a negative value of the paramagnetic Curie–Weiss temperature (θ) (Table I), as well as a deviation of the curve of the ZFC inverse magnetic susceptibility, $1/\chi_{\text{ZFC}}(T)$, downward from its linear portion (Fig. 6). This suggests that the superexchange ferrimagnetic (FIM) long-range below 2 K and antiferromagnetic (AFM) short-range interactions dominate. This may also indicate a higher concentration of paramagnetic neodymium ions in the sample. There was no splitting between the ZFC and FC magnetic susceptibilities for any sample, which suggests no spin frustration in the measured temperature range. The non-zero and temperature-independent contribution of magnetic susceptibility, χ_0 , estimated from the formula [14]

$$\chi T = \frac{C}{1 - \theta/T} + \chi_0 T, \quad (1)$$

with a value of 1.8×10^{-4} emu/mol, is visible only for the sample with $x = 0.0098$ (Fig. 6a).

Magnetic isotherms do not have hysteresis, coercive field, and remanence (Fig. 7). In the reduced coordinate (H/T), the magnetic isotherms fall on a universal Brillouin curve only for $x = 0.0098$. Such behavior is characteristic of superparamagnetic particles. However, with the increase in neodymium ions content in PbNdW samples, isotherms deviate slightly from the universal Brillouin curve. The reason for this is the larger orbital contribution to

the magnetic moment and, consequently, stronger spin-orbit coupling as the factor g decreases with increasing x parameter (Table I).

3.3. Electrical conductivity

The results of electrical measurements of PbNdW sub-microcrystals showed semiconducting behavior of the Arrhenius type in the intrinsic temperature range of 350–400 K with the energy activation of $E_a = 0.73$ eV (Fig. 8). Below 320 K, i.e., in the extrinsic region, a weak activation of the electrical conductivity was observed. Doping with Nd^{3+} ions did not significantly affect the value of electrical conductivity. PbNdW samples obtained after sintering with the same Nd^{3+} concentration turned out to be insulators with electrical conductivity below the measuring level of the instrument.

3.4. Dielectric spectroscopy

Research on broadband dielectric spectroscopy of sub-microcrystalline (Fig. 9) and ceramic (Fig. 10) samples turned out to be very interesting. As already described in Sect. 2.1, the ceramic samples were obtained from sub-microcrystalline ones by sintering. Ceramic samples are more durable and easier to use. The temperature dependencies of the dielectric permittivity, $\varepsilon_r(T)$, and the loss tangent, $\tan(\delta(T))$, of samples with smaller particle size (Fig. 9a–h) and ceramics (Fig. 10a–h) do not differ substantially in shape, but in their values. In both cases, we observe a weak dependence of $\varepsilon_r(T)$ and $\tan(\delta(T))$ on the temperature, frequency, and neodymium ions content below room temperature.

The main difference concerns the dielectric permittivity values, which for ceramics (Fig. 10a–d) are twice higher below 300 K and nine times higher above 300 K than for sub-microcrystalline samples (Fig. 9a–d). In both cases, the energy loss is comparable and small ($\tan(\delta) < 0.05$) below 300 K (Figs. 9e–h and 10e–h) and slightly higher for ceramic samples above 300 K (Fig. 10e–h). The results of $\varepsilon_r(T)$ and $\tan(\delta(T))$ presented studies suggest that the ceramics have a bigger capacity to accumulate charge than the samples before sintering. Interestingly, poor charge accumulation was observed in Pr^{3+} -doped polycrystalline tungstates [15], Gd^{3+} -doped molybdate-tungstates with different grain sizes [4, 5], as well as Mn^{2+} -doped nanocrystalline molybdates [16]. Additionally, strong dipole relaxation above room temperature is observed in the ceramic samples. However, it decreases in both cases with increasing neodymium ions content.

4. Conclusions

The structural, microscopic, magnetic, and electrical studies of nanocrystalline and ceramic samples of the PdNdW solid solution showed that these materials have a scheelite structure and are paramagnetic. Moreover, nanocrystalline samples

show semiconductor properties in the intrinsic region, while ceramic ones are insulators. An important property of ceramic samples is that they have a greater ability to accumulate charge and a strong dipole relaxation above room temperature. This dipole relaxation, however, is strongly suppressed as the neodymium content increases. Up to 300 K, the ceramics under study have a low energy loss and dielectric permittivity independent of temperature, frequency, and neodymium content. For this reason, they can be useful in the manufacture of lossless capacitors.

References

- [1] P. Lecoq, L. Dafinei, E. Auffray, M. Schneegans, M.V. Korzhik, O.V. Mishevitch, V.B. Pavlenko, A.A. Fedorov, A.N. Annenkov, V.L. Kostylev, V.D. Ligon, *Nucl. Instrum. Methods Phys. Res. A* **365**, 291 (1995).
- [2] J.M. Moreau, R.E. Gladyshevskii, P.H. Galez, J.P. Peigneux, M.V. Korzhik, *J. Alloys Compd.* **284**, 104 (1999).
- [3] Y. Huang, H.J. Seo, Q. Feng, S. Yuan, *Mater. Sci. Eng. B* **121**, 103 (2005).
- [4] Z. Kukuła, M. Maciejkowicz, E. Tomaszewicz, S. Pawlus, M. Oboz, T. Groń, M. Guzik, *Ceram. Int.* **45**, 4437 (2019).
- [5] T. Groń, M. Maciejkowicz, E. Tomaszewicz, M. Guzik, M. Oboz, B. Sawicki, S. Pawlus, A. Nowok, Z. Kukuła, *J. Adv. Ceram.* **9**, 40145 (2020).
- [6] S. Gražulis, D. Chateigner, R.T. Downs, A.F.T. Yokochi, M. Quirós, L. Lutterotti, E. Manakova, J. Butkus, P. Moeck, A. Le Bail, *J. Appl. Cryst.* **42**, 726 (2009).
- [7] G.F. Plakhov, M.A. Simonov, E.A. Pobedinskaya, N.V. Belov, *Kristallografiya* **15**, 1067 (1970).
- [8] R. Chipaux, G. André, A. Cousson, *J. Alloys Compd.* **325**, 91 (2001).
- [9] D.M. Trots, A. Senyshyn, B.C. Schwarz, *J. Solid State Chem.* **183**, 1245 (2010).
- [10] X. Yang, J. Huang, *J. Am. Ceram. Soc.* **95**, 3334 (2012).
- [11] J.M. Moreau, Ph. Galez, J.-P. Peigneux, M.V. Korzhik, *J. Alloys Compd.* **238**, 46 (1996).
- [12] H.M. Rietveld, *J. Appl. Cryst.* **2**, 65 (1969).
- [13] J. Rodriguez-Carvajal, *Newsletter of the Commission for Powder Diffraction of the IUCr* **26**, 12 (2001).
- [14] T. Groń, A.W. Pacyna, E. Malicka, *Solid State Phenom.* **170**, 213 (2011).
- [15] T. Groń, M. Piątkowska, E. Tomaszewicz, B. Sawicki, P. Urbanowicz, H. Duda, *Mater. Sci. Pol.* **36**, 530 (2018).
- [16] T. Groń, M. Karolewicz, E. Tomaszewicz, M. Guzik, M. Oboz, B. Sawicki, H. Duda, Z. Kukuła, *J. Nanopart. Res.* **21**, 8 (2019).